FACTA UNIVERSITATIS
Series: **Physics, Chemistry and Technology** Vol. 5, N° 1, 2007, pp. 33 - 44
DOI: 10.2298/FUPCT0701033M

HOMOGENEOUS GAS PHASE MODELS OF RELAXATION KINETICS IN NEON AFTERGLOW

UDC 537.569/.534.8

Vidosav Lj. Marković, Saša R. Gocić, Suzana N. Stamenković

Department of Physics, University of Niš, P.O. BOX 224, 18001 Niš, Serbia

Abstract. *The homogeneous gas phase models of relaxation kinetics (application of the gas phase effective coefficients to represent surface losses) are applied for the study of charged and neutral active particles decay in neon afterglow. The experimental data obtained by the breakdown time delay measurements as a function of the relaxation time* $\overline{t_d}(\tau)$ *(memory curve) is modeled in early, as well as in late afterglow. The number density decay of metastable states can explain neither the early, nor the late afterglow kinetics (memory effect), because their effective lifetimes are of the order of milliseconds and are determined by numerous collision quenching processes. The afterglow kinetics up to hundreds of milliseconds is dominated by the decay of molecular neon* Ne_2^+ *and nitrogen ions* N_2^+ *(present as impurities) and the approximate value of* N_2^+ *ambipolar diffusion coefficient is determined. After the charged particle decay, the secondary emitted electrons from the surface catalyzed excitation of nitrogen atoms on the cathode determine the breakdown time delay down to the cosmic rays and natural radioactivity level. Due to the neglecting of number density spatial profiles, the homogeneous gas phase models give only the approximate values of the corresponding coefficients, but reproduce correctly other characteristics of afterglow kinetics from simple fits to the experimental data.*

Key words: *electrical breakdown, time delay, memory effect, neon afterglow, nitrogen, metastable states, relaxation kinetics, homogeneous gas phase models*

INTRODUCTION

Beginning with 1950s, the memory effect in inert (Ar, Xe) and molecular gases (H_2, N_2) has been reported and explained by the action of the long lived metastable states remaining from the preceding glow [1-4]. The dependence of the mean value of breakdown time delay on the relaxation time $\overline{t_d}(\tau)$ (the memory curve [1-4]) was measured for τ up to 24 hours and therefore, the metastable lifetime of 24 hours was assumed. Moreover, the assumed $Ne(^3P_2)$ ($1s_5$ in Paschen notation) metastable states were quenched by laser light of 614.3*nm* up to about 500*s* in the afterglow at the pressure of 13.3*mbar* [3]. However, it

Received July 13, 2007

should be mentioned that depopulation of $Ne(^3P_2)$ by 588.2*nm* line were studied shorter than 3*ms* in the afterglow [5]. In another paper [6], depopulation of $Ne(^3P_2)$ was examined by laser irradiation tuned to 594.5*nm* shorter than 7*ms* in the afterglow in accordance with our analysis. Namely, this metastable state is quenched very efficiently by numerous collisions with ground state atoms, electrons, walls and between themselves and even elementary considerations show that its effective lifetime is very short on the time scale of the observations of memory effect. The memory curve measurements and metastable hypothesis as an explanation of the memory effect in neon have been repeated in [7-11], neglecting again without justification, the numerous well established quenching processes of metastable states [12], which reduce their effective lifetimes to the order of milliseconds for the pressures and other conditions of those experiments.

The explanation of memory effect in nitrogen and hydrogen based on the decay of metastable states was shown to be incorrect, and therefore a new model was proposed based on surface recombination of nitrogen [13-16] and hydrogen atoms on the cathode [16,17] to provide the secondary electrons for the breakdown initiation. The breakdown time delay measurements was used for nitrogen atom detection down to cosmic rays and natural radioactivity level ($\sim 10^8 cm^{-3}$), as well as the basic laws of surface collision processes were determined: the mechanism and order of surface recombination of nitrogen [13,14,17] and hydrogen atoms [16,17] on different metal surfaces, adsorption isotherm of nitrogen atoms on glass surface, etc.

Following the explanation of the memory effect in the flowing technical purity helium by the surface recombination of nitrogen atoms (present as impurities) [18], this mechanism of secondary electron emission was successfully applied in argon [19] and explained the breakdown time delay variation down to cosmic rays and natural radioactivity level. Therefore, in this paper the measurements are carried out in neon on a gas tube of a similar geometry to that used in previous papers in order to test the metastable, as well as the recombining nitrogen atoms hypotheses. Details of the experimental procedure are shortly summarized in sec. 2, while in sections 3 and 4, the simple analytical and numerical models for the charged and neutral active particles decay are applied and discussed.

2. EXPERIMENTAL DETAILS

The breakdown time delay measurements have been performed for a cylindrical-geometry gas tube made of borosilicate glass also known as "molybdenum sealing glass" (8245, Schott technical glass) with volume of $V \approx 300\ cm^3$ and gold-plated copper cathode (copper rods of 99.98% purity and diameter $D = 6\ mm$, inter-electrode distance $d \approx 6\ mm$). The tube was evacuated down to $10^{-7}\ mbar$, baked at 600 *K*, and then filled with Matheson "research purity" neon at the pressure 6.6 *mbar*, with an nitrogen impurity level below 1 *ppm*. The static breakdown voltage was $U_s = 265\ V$ DC. The time delay measurements were carried out at discharge voltage of $U_W = 400\ V$, glow currents of $I_g = 50\ \mu A$, glow time $t_g = 1\ s$ and relaxation time was varied from very short values up to the saturation range of the memory curve determined by cosmic rays and natural radioactivity. Prior to measurements, the cathode surface was conditioned by running a glow discharge for 30 minutes and several hundreds breakdowns. The mean values of the breakdown delay times were established from series of 100 measurements. During the measurements, the gas tube were protected from light. A personal computer with interface

was used to control the basic parameters of the experiment, and for the acquisition and analysis of data. More details about experimental procedure can be found in [13-17,19].

3. HOMOGENEOUS GAS PHASE MODELS OF METASTABLE AND CHARGED PARTICLES DECAY IN EARLY AFTERGLOW

It is well known that neon atom has two metastable states $Ne(^3P_2)$ and $Ne(^3P_0)$ with very long radiative lifetimes τ_r of 24.4 s and 430 s, respectively [20]. The density of $Ne(^3P_0)$ state is by about one order of magnitude lower than that of $Ne(^3P_2)$ under conditions similar to those of our experiment [12,21,22], therefore only the latter metastable state will be followed in the afterglow. The number density decay of $Ne(^3P_2)$ metastable state in the afterglow is approximately given by:

$$\frac{d[Ne^*]}{d\tau} = -k_a[Ne^*]^2 - k_2[Ne^*][Ne] - k_3[Ne^*][Ne]^2 - D_m/\Lambda^2[Ne^*], \qquad (1)$$

where [Ne*] is the metastable number density, $k_a = 2.5 \times 10^{-10}\ cm^3s^{-1}$ is the rate coefficient for the metastable-metastable collision quenching [23]. The $k_2 = 3.4 \times 10^{-15}\ cm^3s^{-1}$ is the rate coefficient for the two-body quenching in collision with ground-state atom, the $k_3 = 5.0 \times 10^{-34}\ cm^6s^{-1}$ is the rate coefficient for three-body quenching in collision with the two ground state atoms [12]. The last term of equation (1) describes diffusion, followed by quenching processes on the walls with unit probability. The diffusion time constant τ_d can be expressed by $1/\tau_d = D_m/\Lambda^2$, where $D_m = 29.9 cm^2s^{-1}$ [12] is the diffusion coefficient of $Ne(^3P_2)$ metastable state in the parent gas and $\Lambda \approx 1.1 cm$ is the characteristic diffusion length of the tube. The rate coefficient for quenching the metastable states by electrons is very high ($4\times10^{-7}\ cm^3s^{-1}$ [24]), but this process is neglected because the number density of electrons decays very quickly within the first milliseconds in the afterglow. The radiative deexcitation in equation (1) is also neglected because of very long radiative lifetimes [20]. The analytic solution of equation (1), including the aforementioned presumptions, is:

$$[Ne^*] = \frac{[Ne^*]_0 \exp(-\nu_s \tau)}{1 + (k_a/\nu_s)[Ne^*]_0[1 - \exp(-\nu_s \tau)]}, \qquad (2)$$

where $[Ne^*]_0 \approx 3\times10^{11}\ cm^{-3}$ is the initial number density of metastable states at $\tau = 0\,s$ in the afterglow estimated from [21]. The total loss frequency of metastable states defined as $\nu_s = k_2[Ne] + k_3[Ne]^2 + D_m/\Lambda^2$ includes the most important first order loss processes. When the first order processes are predominant $\nu_s >> k_a[\mathrm{Ne}^*]$, the exponential decay of metastable states is obtained:

$$[Ne^*] = [Ne^*]_0\, e^{-\nu_s \tau}. \qquad (3)$$

A review of two and three body quenching rate coefficients of neon metastable states up to early 1976 is given in [25]. However, in Table 1 we have selected from these and later measurements only those where the diffusion coefficient is measured simultaneously with other coefficients. Moreover, Table 1 is extended by the $Ne(^3P_2)$ loss frequencies and effective lifetimes. The diffusion coefficients in Table 1 refer to 6.6 *mbar* and are normalized to the room temperature of 293 *K*. Thus, the total loss frequency for the

$Ne(^3P_2)$ metastable state varies in the range $(604 - 620)s^{-1}$ and will be compared with the total loss frequency determined from our measurements.

Table 1. The diffusion and rate coefficients, the loss frequencies and effective lifetimes for the most important first order processes for $Ne(^3P_2)$ metastable states.

$D_m\left[\frac{cm^2}{s}\right]$	$k_2\left[10^{-15}\frac{cm^3}{s}\right]$	$k_3\left[10^{-34}\frac{cm^6}{s}\right]$	$\nu_s\left[\frac{1}{s}\right]$	$\tau_{eff}\,[ms]$	References
29.9	3.4	5.0	604.5	1.65	[12]
25.3	3.4	6.0	602.7	1.66	[26]
31.9	3.5	4.0	620.1	1.61	[27]

Experimental determination of the loss frequency of metastable states and charged particles

The memory curves $\overline{t_d}(\tau)$ obtained under specified conditions are shown in Fig. 1. We will fit the experimental breakdown time delay data (region I) on the basis of the approximate model and try to establish whether the region I discussed in this section is dominated by metastable and/or charged particle decay. The total breakdown time delay includes the statistical time delay t_s and the formative time t_f, i.e. $t_d = t_s + t_f$ [28]. The mean value of the statistical time delay can be expressed as [28]:

$$\overline{t_s} = 1/YP\,. \tag{4}$$

In equation (4) Y represents a number of generated electrons in the inter-electrode space per second (electron yield), P is the probability of one electron to cause the breakdown and in our conditions $P \approx 0.9$ [13,29]. The statistical fluctuations of the formative time can be neglected [30,31] and therefore the standard deviation of the time delay is $\sigma(t_d) \approx \sigma(t_s) = \overline{t_s}$. Now, the statistical time delay dependence $\overline{t_s}(\tau)$ for the region I in Fig. 1 can be used to follow the metastable and/or charged particle decay in the neon afterglow.

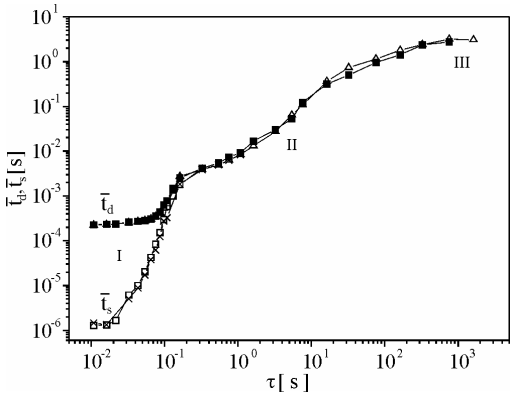

Fig. 1. Memory curves in neon (■ - $\overline{t_d}$ and □ - $\overline{t_s}$ of basic measurements, Δ - $\overline{t_d}$ and ×- $\overline{t_s}$ refer to repeated measurements after 24 hours).

If the breakdown in the region I of the memory curve is initiated by metastable induced secondary electron emission then $Y \propto [Ne^*]$, where $[Ne^*]$ represents the number density of the metastable states in the inter-electrode space. On the other hand, the statistical time delay $\overline{t_s}$ is inversely proportional to the electron yield in the interelectrode space, i.e. $\overline{t_s} \propto (1/Y) \propto (1/[Ne^*])$. If we show $\overline{t_s}$ as a function of τ in a semi-log scale, the dependence is linear (Fig. 2) confirming the assumed first order decay in this afterglow period, which is consistent both with ion and metastable mechanisms. In order to distinguish between these two mechanisms we must consider the effective lifetimes of metastable states.

In this approximate gas phase model the electron yield in the inter-electrode space is given by:

$$Y = \gamma_m \frac{[Ne^*]\bar{v}}{4} S_C , \tag{5}$$

where γ_m is the secondary electron yield by metastable collision, $\bar{v} = 5.5 \times 10^4\ cms^{-1}$ is the mean thermal velocity and $S_C = 0.28\ cm^2$ the front area of the cathode surface. By combining the equations (3), (4) and (5), the loss frequency ν_s is obtained as:

$$\nu_s = \frac{\ln(\overline{t_s} / \overline{t_{s0}})}{\tau}, \tag{6}$$

where $\overline{t_{s0}}$ is the intercept on the ordinate axis. If $\overline{t_s}(\tau)$ for the region I is presented in the semi-log scale, the dependence is linear confirming that the principal process that controls the breakdown is of the first order in this afterglow period (Fig. 2). From relation (6) and $\overline{t_s}$, $\overline{t_{s0}}$ and τ taken from Fig. 2, the experimental loss frequency is obtained $\nu_s \approx 62\ s^{-1}$ and therefore, the experimental effective lifetime is $\tau_{eff} = 1/\nu_s \approx 16\ ms$. For the coefficients cited in Table 1, the metastable loss frequencies are greater by about 10 times than the experimental value, even though some quenching processes were neglected in the model. Therefore, we may conclude that the afterglow is dominated by other

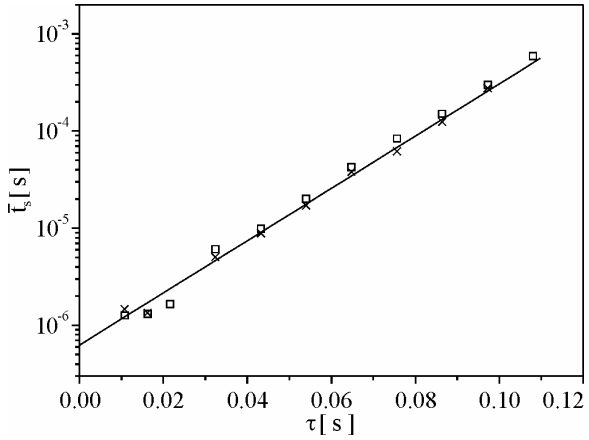

Fig. 2. Statistical time delay of basic measurements (□) and of repeated measurements (×) and least-square fit (solid line).

particles, not metastables. In paper [4], where the memory effect was observed at the pressure 40 *mbar*, a discrepancy between the assumed metastable lifetimes in [1-4,7-11] and the calculated one from our analysis is even greater, although we use the smallest coefficients from [26]. At the pressure 40 *mbar*, the total loss frequency is $\nu_s \sim 3950\ s^{-1}$ and $\tau_{eff} \sim 0.25\ ms$, showing that metastable states are not the carriers of the memory effect lasting of minutes or even hours.

If the breakdown is initiated by ions in the region I of the memory curve, than the diffusion time constant τ_i is $\tau_i = \Lambda^2/D_{eff}$, where D_{eff} is the effective ion diffusion coefficient in this afterglow period. With $\tau_i = \tau_{eff} \approx 16\ ms$ determined from $\overline{t_s}(\tau)$ curve (Fig. 2), it follows that $D_{eff} \approx 73\ cm^2 s^{-1}$, which is approximately equal to the ambipolar diffusion coefficient of nitrogen N_2^+ ions present as impurities in neon ($D_{an} = 70\ cm^2 s^{-1}$ [32]). According to exact numerical calculations based on the macrokinetic diffusive model in realistic geometry of the tube [33], the best fit of the experimental data is obtained with 0.3 *ppm* nitrogen impurities in neon. Assuming this level of nitrogen impurity, we will apply a homogeneous gas phase numerical model in order to follow the metastable and charged particle decay in neon afterglow.

Homogeneous gas phase model of metastable and charged particle decay in neon afterglow - numerical solution

The decay of the $Ne(^3P_2)$ metastable state and Ne^+, Ne_2^+ and N_2^+ ions in neon afterglow can be followed by numerically solving the system of four ordinary differential equations (7-10) and for the electron yield in the inter-electrode space (11):

$$\frac{\partial[Ne^*]}{\partial\tau} = -(D_m/\Lambda^2)[Ne^*] - k_a[Ne^*]^2 - k_e[Ne][Ne^*] - k_2[Ne^*][Ne] - k_3[Ne^*][Ne]^2 + k_r[Ne_2^+][Ne], \tag{7}$$

$$\frac{\partial[Ne^+]}{\partial\tau} = -k_c\,[Ne^+][Ne]^2 + k_a[Ne^*]^2 - (D_{a1}/\Lambda^2)\,[Ne^+], \tag{8}$$

$$\frac{\partial[Ne_2^+]}{\partial\tau} = k_c[Ne^+][Ne]^2 - k_r[Ne_2^+][Ne] - k_{cn}[Ne_2^+][N_2] - (D_{a2}/\Lambda^2)[Ne_2^+], \tag{9}$$

$$\frac{\partial[N_2^+]}{\partial\tau} = k_{cn}[Ne_2^+][N_2] - k_{rn}[N_e][N_2^+] - (D_{an}/\Lambda^2)[Ne_2^+] \tag{10}$$

$$Y = C\cdot\{\gamma_{i2}[Ne_2^+]\,S_C\overline{v_{i2}}/4 + \gamma_{i2}[Ne_2^+]\,S_C w_{i2} + \gamma_{in}[N_2^+]\,S_C\overline{v_{in}}/4 + \gamma_{in}[N_2^+]\,S_C w_{in}\}, \tag{11}$$

where C is the proportionality constant, including the factors related to electrode geometry, electron distributions, etc. The first term in equation (7) designates the diffusion of the metastable states to the tube walls, with the diffusion coefficient D_m [12]. The two- and three- body collision quenching rate coefficients k_2 and k_3, respectively are also taken from [12] and shown in Table 1. For the metastable quenching in electron collisions a value $k_e = 4\times10^{-7}\ cm^3 s^{-1}$ was used from [24] with an assumption that $[N_e] \approx [Ne^+]$, for

the dissociative recombination of molecular neon ions $k_r = 1.8 \times 10^{-7}\, cm^3 s^{-1}$ [34] and of nitrogen ions $k_m = 2 \times 10^{-7}\, cm^3 s^{-1}$ [35] (the second terms of (9) and (10), respectively). The first terms of equations (8,9) describe the termolecular ion-neutral association reaction in collisions of atomic neon ion with two ground state atoms:

$$Ne^+ + 2Ne \rightarrow Ne_2^+ + Ne \tag{12}$$

with the rate coefficient $k_c = 4.4 \times 10^{-32}\, cm^6 s^{-1}$ [36]. The first term of equation (10) describe the production of N_2^+ ions from asymmetric charge transfer reaction in collisions of molecular neon ion with nitrogen molecule:

$$Ne_2^+ + N_2 \rightarrow N_2^+ + 2Ne \tag{13}$$

with the rate coefficient $k_{cn} = 9.1 \times 10^{-10}\, cm^3 s^{-1}$ [37]. In equation (11) we use the following notation: γ_{i2}, γ_{in} are the secondary electron yields caused by molecular neon and nitrogen ions, respectively; $w_{i2} = 2.6 \times 10^5\, cms^{-1}$ [38] and $w_{in} = 1 \times 10^5\, cms^{-1}$ [39] are their drift velocities to the cathode after the application of voltage and $\overline{v_{i2}} = 3.9 \times 10^4\, cms^{-1}$ and $\overline{v_{in}} = 4.7 \times 10^4\, cms^{-1}$ are their mean thermal velocities. The last terms on the right hand side of (8-10) designate diffusion of $[Ne^+]$, $[Ne_2^+]$ and $[N_2^+]$ ions, with the ion diffusion coefficients in our conditions $D_{a1} = 32\, cm^2 s^{-1}$ [40,32], $D_{a2} = 47.2\, cm^2 s^{-1}$ [41] and $D_{an} = 70\, cm^2 s^{-1}$ [32], respectively. The initial number density of atomic ions is estimated from the Poisson equation $[Ne^+]_0 \approx \varepsilon_0 U_{CF} / e d_{CF}^{\,2} \approx 2.3 \times 10^{10}\, cm^{-3}$, where ε_0 is the permittivity constant, $U_{CF} \approx 400\, V$ is the voltage drop in the cathode fall and $d_{CF} \approx 0.15\, cm$ its width. The initial number density of molecular ions is assumed to be $[Ne_2^+]_0 \approx 7 \times 10^9\, cm^{-3}$ (30% of number density of atomic ions [22,26]) and $[N_2^+]_0 \approx 7 \times 10^8\, cm^{-3}$ (not important for the calculation, as demonstrated in Figs 3,4).

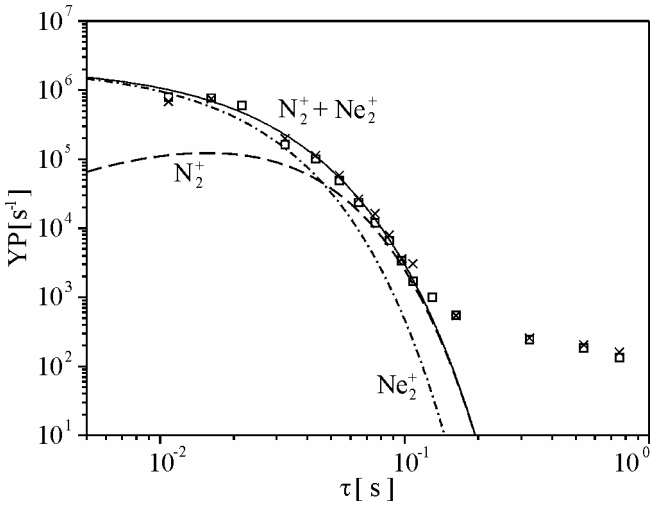

Fig. 3. Experimental data for the region I fitted by N_2^+ (dashed line) decay and Ne_2^+ (dash-dot line) decay. Solid line is the sum of N_2^+ and Ne_2^+ contributions.

The system of ordinary differential equations (7-11), representing the homogeneous gas phase model of afterglow kinetics in neon, is solved by using fourth-order Runge-Kutta method. The fitting parameters are adjusted in order to fit the experimental data. Best fit of experimental data (Fig. 3) is obtained for $C\gamma_{i2} = 3.9 \times 10^{-9}$ and $C\gamma_{in} = 2.6 \times 10^{-9}$. The fitting parameters in this model give only apparent secondary electron yields due to the neglecting of number density spatial profiles (calculated in diffusive model [33]). It is clear from Figs 3, 4 that only the decay of molecular neon Ne_2^+ and nitrogen N_2^+ ions can fit the experimental data for the electron yield versus τ and explain the early memory effect in neon. In the early afterglow, due to termolecular ion-neutral association reaction (12), the number density of atomic ions is very fast depleted (Fig. 4, dotted line). After that, the molecular neon Ne_2^+ originating from aforementioned termolecular ion-neutral association reaction (12) and nitrogen N_2^+ ions originating from asymmetric charge transfer reaction (13), are dominant (Fig. 4, dash-dot and solid line, respectively). On the other hand, the metastable states have a very fast decrease and cannot fit the slope of experimental data (Fig. 4, dashed line), in accordance with the preceding conclusion that metastable states are not carriers of the memory effect.

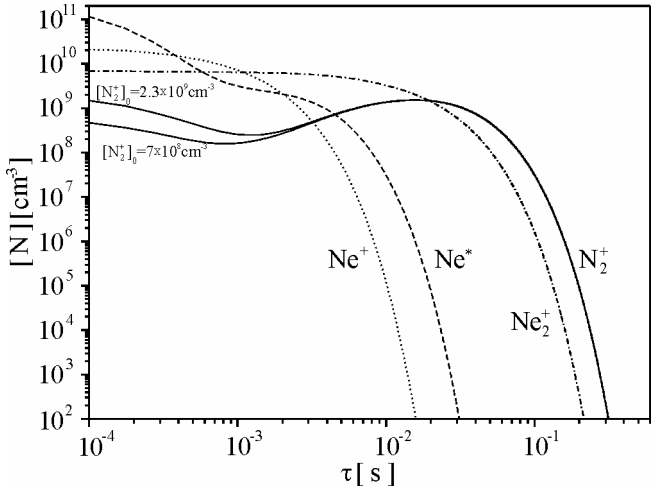

Fig. 4. Decay of number densities in neon afterglow: atomic neon ions Ne^+ (dotted line), metastable states Ne^* (dashed line), molecular neon ions Ne_2^+ (dash-dot line) and molecular nitrogen ions N_2^+ with different initial number densities (solid lines).

5. HOMOGENEOUS GAS PHASE ODEL OF NEON LATE AFTERGLOW (REGIONS II AND III OF THE MEMORY CURVE)

The number density decay of metastable states can explain neither the early nor the late memory effect in neon and now we will test the surface recombination of nitrogen atoms present as impurities, as it done in helium [18] and argon [19]. The effect of the surface-catalyzed excitation was reported in [42-45], when it was discovered that electronically excited molecules of nitrogen could be formed by recombination of N atoms on certain metal surfaces, such as nickel, cobalt, copper and silver. Spectroscopic

and photographic analyses indicate formation of $N_2(A^3\Sigma_u^+)$ metastables states on the metal surfaces [42-45]. The main loss processes of nitrogen atoms in the neon afterglow are the recombination on the glass walls and the surface recombination of atoms on electrodes with or without forming excited molecules is responsible for production of secondary electrons and initiation of breakdown. In the homogeneous gas phase representation of surface losses, the loss rates of the density of nitrogen atoms during the afterglow and the electron yields are given by equations [14,46,47]:

$$\frac{d[N]}{d\tau} = -\gamma_{nw}[N]^2, \tag{14}$$

$$Y_N = \gamma_1^{eff}[N]V_C + \gamma_2^{eff}[N]^2 V_C + Y_0, \tag{15}$$

where γ_{nw} designates the effective gas phase rate coefficient for the second order surface recombination on glass walls, V_C is the volume of the inter-electrode space, Y_0 is the "background" electron yield and γ_1^{eff}, γ_2^{eff} are the effective gas phase rate coefficients for the surface recombination on the cathode and are first and second order, respectively. These rate coefficients in (14) and (15) are defined in relation to the gas phase number density of nitrogen atoms and are frequently encountered in the literature [13,14,46,47]. The plateau of the saturation region III (Fig. 1) is determined by the cosmic rays and natural radioactivity level and is used to determine "background" electron yield as $Y_0 \approx 1/\left(\overline{t_d^{sat}}\, P\right) \approx 0.4\ s^{-1}$. The initial number density of nitrogen atoms are assumed to be

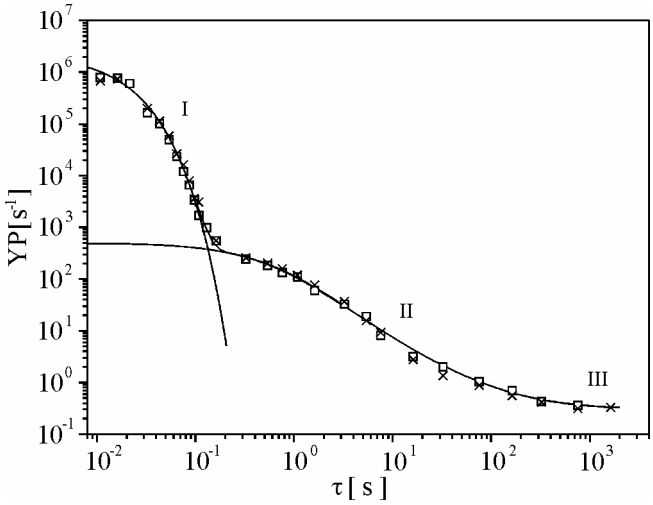

Fig. 5. Fitting of experimental data by the homogeneous gas phase models (□, × - refer to basic and repeated measurements, respectively).

$[N]_0 = 9.6 \times 10^9\ cm^{-3}$ which corresponds to about 0.3 *ppm* impurity content of nitrogen in neon and degree of dissociation of ~ 10%. Degree of dissociation was found to increase when the fraction of nitrogen in rare gases decreases [48-52], and typical value is of the order of ~ 10%. The best fit for the region II of the memory curve is obtained for

$\gamma_{nw} = 1.3\times10^{-10}\ cm^3s^{-1}$, $\gamma_1^{eff} = 4.2\times10^{-8}\ s^{-1}$ and $\gamma_2^{eff} = 3\times10^{-17}\ cm^3s^{-1}$ (Fig. 5, the right solid line). The effective coefficients γ_1^{eff} and γ_2^{eff} include the probability of secondary electron emission through the adsorbed layer of neon atoms, as well as all other factors not considered in the model. As for the estimation of the initial nitrogen atom number density in the afterglow, the conjugation relation holds $\gamma_{nw}[N_0] = const$, which means that if $[N_0]$ increases, γ_{nw} decreases (as well as γ_1^{eff} and γ_2^{eff}), and vice versa. Also, a support of the recombination hypothesis is the observation of afterglow in Xe and Kr with small amount of nitrogen. The afterglow was followed to ten seconds in Xe [53] and author proposed nitrogen metastable states and nitrogen atoms as a source of energy storage.

6. CONCLUSION

The breakdown time delay measurements are efficient method for the study of gas phase and surface processes accompanied by the approximate gas phase and more exact diffusive models. The fits of experimental data based on application of the gas phase effective coefficients to represent surface losses, give only the approximate values of the recombination coefficients due to the neglecting of number density spatial profiles, but determine correctly the mechanism of breakdown initiation, as well as the order of dominant afterglow processes.

The metastable hypothesis frequently used in the literature [1-4,7-11], completely failed to explain the memory effect in neon by the action of long-lived metastable states remaining from the preceding glow. These authors have neglected the numerous quenching processes of metastable states in collisions with ground state atoms, electrons, walls and between themselves, which reduce their effective lifetimes down to the order of milliseconds under the conditions of those experiments. It was found that the afterglow kinetics up to hundreds of milliseconds is dominated by the decay of molecular neon ions Ne_2^+ (originating from termolecular Ne^+ ion-neutral association reaction) and than by the decay of molecular nitrogen ions N_2^+ (originating from asymmetric charge transfer reaction in collisions with Ne_2^+). After that, nitrogen atoms recombining on the cathode surface determine the breakdown time delay dependence down to the cosmic rays and natural radioactivity level. Thus, the quantitative explanation of the memory effect was given based on the homogeneous gas phase models for representation of surface loses in early, as well as in late neon afterglow.

Acknowledgments. *Authors are grateful to MNŽZS of Serbia for partial support (project 141025).*

REFERENCES

1. Đ. A. Bošan, Proc. 5th Int. Conf. on Gas Discharges (Liverpool University, Liverpool, UK, 1978) pp. 273-276
2. Đ. A. Bošan and M. M. Pejović, J. Phys. D: Appl. Phys. **12**, 1699 (1979)
3. Đ. A. Bošan, M. K. Radović and Đ. M. Krmpotić, J. Phys. D: Appl. Phys. **19**, 2343 (1986)
4. Đ. A. Bošan and T. V. Jovanović, J. Phys. D: Appl. Phys. **25**, 436 (1992)
5. F. C. M. Coolen, N. van Schaik L. W. G. and Steenhuijsen, Physica **93**, 253 (1978)

6. A. D. Ernest, S. C. Haydon and W. Yumin W, J. Phys. D: Appl. Phys. **25**, 1187 (1992)
7. M. M. Pejović, G. S. Ristić and J. P. Karamarković, J. Phys. D: Appl. Phys. **35**, R91 (2002)
8. I. V. Spasić, M. K. Radović, M. M. Pejović and ·Č. A. Maluckov, J. Phys. D: Appl. Phys. **36**, 2515 (2003)
9. Č. A. Maluckov and M. K. Radović, IEEE Trans. Plasma Sci. **30**, 1597 (2002)
10. Č. A. Maluckov, J. P. Karamarković, M. K. Radović and M. M. Pejović, Physics of Plasmas **11**, 5328 (2004)
11. M. M. Pejović and Mi. M. Pejović, Plasma Sources Sci. Technol. **14**, 492 (2005)
12. A. V. Phelps, Phys. Rev. **114**, 1011 (1959)
13. V. Lj. Marković, Z. Lj. Petrović and M. M. Pejović, J. Chem. Phys. **100**, 8514 (1994)
14. V. Lj. Marković, M. M. Pejović and Z. Lj. Petrović, Plasma. Chem. Plasma Process. **16**, 195 (1996)
15. V. Lj. Marković, Z. Lj. Petrović and M. M. Pejović, Plasma Sources Sci. Technol. **6**, 240 (1997)
16. V. Lj. Marković, M. M. Pejović, Z. Lj. Petrović and S. S. Manola, Proc. 3rd General Conference of the Balkan Physical Union (Cluj-Napoca, Romania, 1997), published in Balkan Phys. Lett. 5, 133 (1997)
17. Z. Lj. Petrović, V. Lj. Marković, M. M. Pejović and S. R. Gocić, J. Phys. D: Appl. Phys. **34**, 1756 (2001), and references therein
18. V. Kudrle, E. LeDuc and M. Fitaire M, J. Phys. D: Appl. Phys. **32**, 2049 (1999)
19. V. Lj. Marković, S. R. Gocić, S. N. Stamenković and Z. Lj. Petrović, Physics of Plasmas **12**, 073502 (2005)
20. N. E. Small-Warren and L. Y. Chiu, Phys. Rev. A **11**, 1777 (1975)
21. Y. Ichikawa and S. Teii, J. Phys. D: Appl. Phys. **13**, 1243 (1980)
22. Y. Ichikawa and S. Teii, J. Phys. D: Appl. Phys. **13**, 2031 (1980)
23. N. Winter, C. Bender and T. Rescigno, J. Chem. Phys. **67**, 3122 (1977)
24. V. I. Demidov and N. B. Kolokolov, J. Tech. Phys. **48**, 1832 (1978)
25. M. F. Golde, in *Gas Kinetics and Energy Transfer*, Volume 2 (The Chemical Society, Burlington House, London, 1977)
26. L. W. G. Steenhuijsen, Beitr. Plasmaphys. **21**, 301 (1981)
27. K. Tachibana, H. Harima and Y. Urano Y, Jpn. J. Appl. Phys. **21**, 1529 (1982)
28. Morgan C G, in *Electrical Breakdown of Gases* edited by J. M. Meek and J. D. Craggs (John Wiley & Sons, Chichester, 1978)
29. V. Lj. Marković, S. R. Gocić, S. N. Stamenković, Z. Lj. Petrović and M. Radmilović, Eur. Phys. J. AP **14**, 171 (2001)
30. V. Lj. Marković, S. R. Gocić, and S. N. Stamenković, J. Phys D: Appl. Phys. **39**, 3317 (2006)
31. V. Lj. Marković, S. N. Stamenković, S. R. and Gocić, Eur. Phys. J. AP **38**, 73 (2007)
32. T. D. Märk and H. J. Oskam, Z. Physik **247**, 84 (1971)
33. V. Lj. Marković, S. R. Gocić, S. N. Stamenković and Z. Lj. Petrović, to be published
34. W. H. Kasner, Phys. Rev. **167**, 148 (1968)
35. M. Geoghegan, N. G. Adams and D. Smith, J. Phys. B: At. Mol. Opt. Phys. **24**, 2589 (1991)
36. A. P. Vitols and H. J. Oskam, Phys. Rev. A **5**, 2618, (1972)
37. D. K. Bohme, N. G. Adams, M. Mosesman, A. B. Dunkin A B and E. E. Ferguson, J. Chem. Phys. **52**, 5094 (1970)
38. A. von Engel, *Electric Plasmas: Their Nature and Uses* (Taylor & Francis Ltd, London and New York, 1983)
39. H. W. Ellis, R. Y. Pai, E. W. McDaniel, E. A. Mason and L. A. Viehland, At. Data and Nucl. Data Tables **17**, 177 (1976)
40. E. W. Mc Daniel and E. A. Mason, *The Mobility and Diffusion of Ions in Gases* (John Wiley and Sons, New York, 1973)
41. C. E. Beaty and P. L. Patterson, Phys. Rev. **137**, 116 (1968)
42. R. R. Reeves, G. G. Manella and P. Harteck, J. Chem. Phys. **32**, 946 (1960)
43. G. G. Mannella and P. Harteck, J. Chem. Phys. **34**, 2177 (1961)
44. G. G. Mannella, R. R. Reeves and P. Harteck, J. Chem. Phys. **33**, 636 (1960)
45. P. Harteck, R. R. Reeves and G. G. Manella, Can. J. Chem. **38**, 1648 (1960)
46. V. Lj. Marković, Z. Lj. Petrović and M. M. Pejović, J. Phys. III **6**, 959 (1996)
47. V. Lj. Marković, S. R. Gocić and S. N. Stamenković, *Statistically Based Methods in the Physics of Ionized Gases* (Faculty of Natural Sciences and Mathematics, Niš, 2004) (in serbian)
48. N. Sasaki, Y. Uchida and M. Shoi M, Proc. 16th European Sectional Conference on the Atomic and Molecular Physics of Ionized Gases (Grenoble, France, 2002) pp. 217-218
49. P. A. Sa and J. Loureiro, J. Phys. D: Appl. Phys. **30**, 2320 (1997)
50. A. Ricard, A. Besner, J. Hubert and M. Moisan, J. Phys. B: At. Mol. Opt. Phys. **21**, L579 (1988)
51. T. Kimura and K. Ohe, Jpn. J. Appl. Phys. **31**, 4051 (1992)
52. T. Kimura, K. Akatsuka and K. Ohe, J. Phys. D **27**, 1664 (1994)
53. C. Kenty, J. Chem. Phys. **47**, 2545 (1967)

HOMOGENI GASNO FAZNI MODELI RELAKSACIONE KINETIKE U NEONU

Vidosav Lj. Marković, Saša R. Gocić, Suzana N. Stamenković

U ovom radu koriste se homogeni gasno fazni modeli relaksacione kinetike (tj. opisivanje površinskih gubitaka primenom efektivnih gasno faznih koeficijenata) za proučavanje raspada naelektrisanih i neutralnih aktivnih čestica u neonu. Modelovani su eksperimentalni podaci dobijeni merenjem vremena kašnjenja električnog proboja u funkciji vremena relaksacije (memorijska kriva). Pokazano je da hipoteza sa metastabilnim stanjima ne može objasniti memorijski efekat zbog vrlo kratkog efektivnog vremena života metastabilnih stanja (reda milisekundi u datim uslovima) određenog brojnim sudarnim procesima. Memorijski efekat do stotinu milisekundi je opisan raspadom molekulskih jona neona Ne_2^+ i azota N_2^+ (prisutnog kao nečistoća) i približno je određena vrednost koeficijenta ambipolarne difuzije jona azota N_2^+. Nakon raspada naelektisanih čestica pa do nivoa kosmičkog zračenja i prirodne radioaktivnosti okoline, vreme kašnjenja proboja je određeno sekundarnom emisijom elektrona na osnovu energije površinski katalizovane rekombinacije atoma azota na katodi. Zbog zanemarivanja prostornih profila koncentracija, homogeni gasno fazni modeli daju samo približne vrednosti rekombinacionih koeficijenata, ali korektno reprodukuju ostale karakteristike relaksacione kinetike na osnovu jednostavnog fita eksperimentalnih podataka.